materials

MDPI

Article

Two Magnetic Orderings and a Spin–Flop Transition in Mixed Valence Compound $Mn_3O(SeO_3)_3$

Wanwan Zhang [1], Meiyan Cui [2], Jindou Tian [3], Pengfeng Jiang [1], Guoyu Qian [1,*] and Xia Lu [1]

[1] School of Materials, Sun Yat-sen University, Guangzhou 510275, China
[2] State Key Laboratory of Structural Chemistry, Fujian Institute of Research on the Structure of Matter, Chinese Academy of Sciences, Fuzhou 350002, China
[3] Department of Chemistry, University of Science and Technology of China, Hefei 230026, China
* Correspondence: qiangy@mail.sysu.edu.cn

Abstract: A mixed-valence manganese selenite, $Mn_3O(SeO_3)_3$, was successfully synthesized using a conventional hydrothermal method. The three-dimensional framework of this compound is composed of an MnO_6 octahedra and an SeO_3 trigonal pyramid. The magnetic topological arrangement of manganese ions shows a three-dimensional framework formed by the intersection of octa-kagomé spin sublattices and staircase-kagomé spin sublattices. Susceptibility, magnetization and heat capacity measurements confirm that $Mn_3O(SeO_3)_3$ exhibits two successive long-range antiferromagnetic orderings with T_{N1}~4.5 K and T_{N2}~45 K and a field-induced spin–flop transition at a critical field of 4.5 T at low temperature.

Keywords: mixed-valence; magnetic properties; topological structures

check for updates

Citation: Zhang, W.; Cui, M.; Tian, J.; Jiang, P.; Qian, G.; Lu, X. Two Magnetic Orderings and a Spin–Flop Transition in Mixed Valence Compound $Mn_3O(SeO_3)_3$. *Materials* **2022**, *15*, 5773. https://doi.org/10.3390/ma15165773

Academic Editor: Emil Babić

Received: 7 July 2022
Accepted: 18 August 2022
Published: 21 August 2022

Publisher's Note: MDPI stays neutral with regard to jurisdictional claims in published maps and institutional affiliations.

Copyright: © 2022 by the authors. Licensee MDPI, Basel, Switzerland. This article is an open access article distributed under the terms and conditions of the Creative Commons Attribution (CC BY) license (https://creativecommons.org/licenses/by/4.0/).

1. Introduction

Mixed valence transition metal (TM) oxides with three-dimensional electronic configurations are of great significance in the fields of materials chemistry, electrochemical energy and condensed matter physics due to their diverse crystal structures and electronic configurations [1,2]. From the ancient application of Fe_3O_4 in the compass to today's copper-based high temperature superconducting materials, mixed valence TM oxides exhibit exciting and unusual chemical and physical behaviors, including high-temperature superconductors [3], colossal magnetoresistance [4], ion deintercalation [5], metal-insulator transition [6], electrocatalysis/photocatalysis [7,8], etc. More specifically, copper oxides with bidimensional characters, together with the mixed valency of Cu^+/Cu^{2+} or Cu^{2+}/Cu^{3+}, are responsible for superconducting properties [9,10]. The ferromagnetic (FM) material $La_{0.67}Sr_{0.33}MnO_3$ exhibits metallic conductivity due to the Zener double exchange mechanism between Mn^{3+} and Mn^{4+} ions, but $BaFe_{12}O_{19}$ (also an FM material) is insulative due to the limitation of the ratio of Fe^{2+} and Fe^{3+} ions [11]. Compound $K_2Cr_8O_{16}$ (hollandite), with a rare Cr^{3+}/Cr^{4+} mixed valence state, exhibits a metal-insulator transition in a FM state [12]. The transition metal valence state of cathode material $LiMO_2$ (M = Mn, Co, Ni) will switch back and forth between M^{2+} and M^{4+} during charging and discharging processes in Li-ion batteries [13,14]. X. Yu et al. reported the experimental observation of skyrmionic bubbles with various topological lattices in colossal magnetoresistive manganite $La_{1-x}Sr_xMnO_3$ [15]. In order to discover new materials with unusual physical/chemical properties, it is necessary to explore new mixed-valence transition metal compounds. The compound $Mn_3O(SeO_3)_3$ ($Mn^{II}Mn^{III}{}_2O(SeO_3)_3$) was first reported by Wildner [16]. Structure analysis confirmed that this compound shows a channel structure with a three-dimensional magnetic topological framework formed by the intersection of octa-kagomé spin sublattices and staircase-kagomé spin sublattices; however, there are few studies regarding its magnetic properties. In this paper, we report the discovery of a mixed valence manganese selenate $Mn_3O(SeO_3)_3$.

Magnetic measurements indicate that this compound possesses two successive antiferromagnetic (AFM) transitions at low-temperature. Moreover, a spin–flop transition is observed at 2 K with an applied magnetic field of ~4.5 T.

2. Experimental Section

2.1. Synthesis of $Mn_3O(SeO_3)_3$

Single crystals of $Mn_3O(SeO_3)_3$ were obtained using a conventional hydrothermal method. A mixture of 2 mmol $Mn(NO_3)_2 \cdot xH_2O$ (3 N, 0.3943 g), 2 mmol LiI (2 N, 0.2704 g), 1 mmol SeO_2 (4 N, 0.1110 g) and 5 mL deionized water was sealed in an autoclave equipped with a Teflon liner (28 mL). The autoclave was gradually heated to 230 °C at a rate of 1 °C/min, held for 4 days and then naturally cooled to room temperature. The product contained the desired black noodle-like crystals with a 90% yield. The crystals' sizes and morphologies were characterized using a stereomicroscope and field emission scanning electron microscopy (FE-SEM, SU8100, Hitachi, Tokyo, Japan). Figure S1 shows images of the crystals under the stereomicroscope and FE-SEM. It can be observed that the crystal size is approximately 0.3 × 0.08 × 0.05 mm. The product's impurities were manually removed under a microscope. Powdered samples were prepared for physical measurement by crushing small single crystals; purity was confirmed by powder X-ray diffraction (XRD) analysis (Figure 1). Moreover, the reagent LiI acted as a mineralizer, as the quality of crystals was unsatisfactory without it.

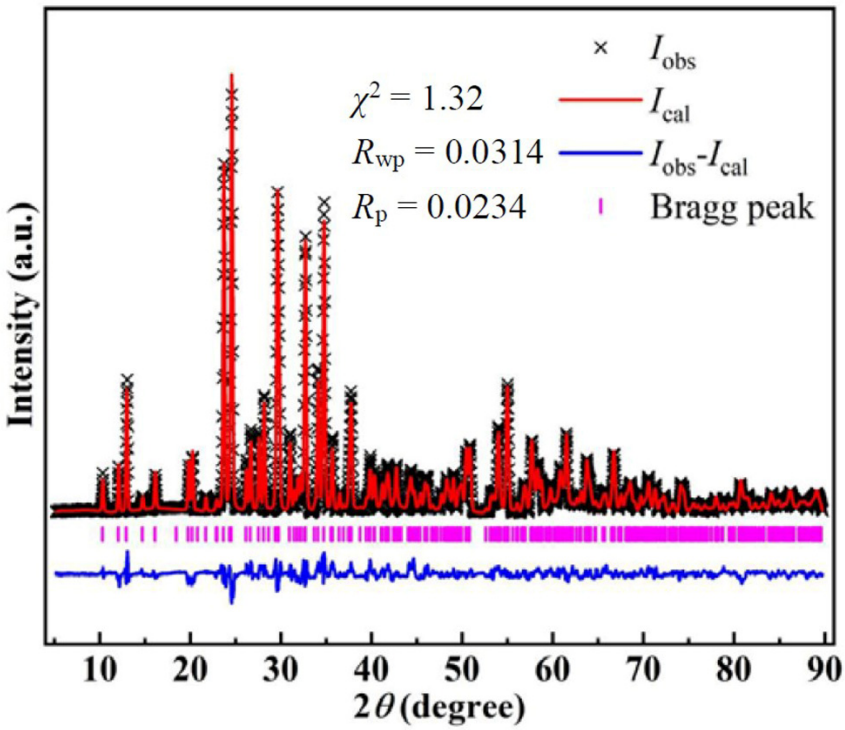

Figure 1. Rietveld refinement of powder X-ray (Cu Kα) diffraction patterns for $Mn_3O(SeO_3)_3$. The refined lattice constants are a = 15.484(9) Å, b = 6.665(8) Å, c = 9.703(1) Å and β = 118.79(4)° with space group $C2/m$, which is consistent with the reported parameters of ref. [16].

2.2. Methods

XRD patterns were collected using a Bruker D8 diffractometer with Cu-K_α radiation (λ~1.5418 Å) at room temperature. Rieltveld refinement was performed using GSAS-EXPGUI software [17]. Refined crystal structures were analyzed using VESTA software [18]. Furthermore, element analysis was observed using FE-SEM with an X-ray energy-dispersive spectrometer (EDS). EDS analysis confirmed the molar ratio of Mn/Se as 3.1/2.0, which is in good agreement with the X-ray structure analysis. Thermogravimetric

analysis (TGA) of $Mn_3O(SeO_3)_3$ was collected on NETZSCH STA 449C instruments with an Al_2O_3 crucible from 50 to 900 °C at a rate of 10 °C/min under N_2 atmosphere.

Magnetic measurements of a powdered sample of $Mn_3O(SeO_3)_3$ were performed using a PPMS (Quantum Design, San Diego, CA, USA). The powdered sample (20.6 mg) was placed in a plastic capsule, which was suspended in a copper tube slot. Magnetic susceptibility was measured at 0.1 T from 2 to 300 K. Magnetization was measured at different temperatures at applied field from 0 to 9 T. Heat capacity was measured with the same PPMS system at zero field and determined using a relaxation method on a 5.6 mg sample.

3. Results and Discussion

The structure of compound $Mn_3O(SeO_3)_3$ was first reported by Wildner [16]. $Mn_3O(SeO_3)_3$ crystallizes in the monoclinic system with the space group $C2/m$. As shown in Figure S2, both Mn and Se atoms have three crystallographic sites. The oxidation state is +2 for Mn1 and +3 for Mn2/Mn3. All manganese atoms are coordinated by six oxygen atoms forming MnO_6 distorted octahedra; Mn–O bond lengths range from 2.100(1) to 2.361(8) Å for $Mn1^{2+}O_6$ octahedra and from 1.854(2) to 2.310(6) Å for $Mn2^{3+}O_6$ and $Mn3^{3+}O_6$, respectively. In other words, the degree of distortion for $Mn1^{2+}O_6$ octahedra is smaller than that of $Mn2^{3+}O_6$ and $Mn3^{3+}O_6$. This is due to the Mn^{3+} ($t_{2g}^3e_g^1$) octahedron with a remarkable Jahn–Teller effect, which may induce a larger structure distortion than Mn^{2+} ($t_{2g}^3e_g^2$). All selenium atoms are in trigonal pyramid geometry with a stereoactive lone pair of 4 s^2 in Se^{4+} ions; the Se-O bond lengths are approximately 1.70 Å. It should be noted that Se1/Se2/Se3 atoms are surrounded by 4/5/6 manganese atoms with a Se-O-Mn route, respectively. These 4/5/6 manganese atoms contain two Mn^{2+} atoms and 2/3/4 Mn^{3+} atoms, respectively.

As shown in Figure 2, $Mn_3O(SeO_3)_3$ shows a tunnel structure along the b-axis, in which the framework is constituted by MnO_6 octahedra and SeO_3 trigonal pyramids. $Mn1O_6$ octahedra share their edges (O5–O6) to form uniform [-Mn1-] chains along the b-axis. $Mn^{3+}O_6$ octahedra are interconnected via edge-sharing oxygen atoms, forming a two-dimensional [-Mn^{3+}-] layered structure parallel to (001). The detailed linkage mode between manganese ions is shown in Figure 3. Two $Mn2O_6$ octahedra connect to each other by edge-sharing oxygen atoms (O4–O4) to form a [Mn_2O_{10}] dimer along the a-axis. The Mn2-O4-Mn2 angle is 101.34(9)°. $Mn3O_6$ octahedra are interconnected by corner-sharing oxygen atoms (O7) to form uniform [-Mn3-] chains along the b-axis. One $Mn2O_6$ octahedron and two $Mn3O_6$ octahedra are connected in an isosceles triangle configuration. The neighbored [-Mn^{3+}-] layers are separated by [-Mn1-] chains and SeO_3 trigonal pyramids. Furthermore, we noted that $Mn1O_6$ octahedra are interconnected with $Mn2O_6$ octahedra via conner-sharing O5 atoms, but $Mn1O_6$ and $Mn3O_6$ octahedra are connected by SeO_3 groups in the manner of Mn1-O-Se-O-Mn3. After removing the nonmagnetic SeO_3^{2-} groups, the topological arrangement of magnetic Mn ions is a three-dimensional framework (Figure 2b). Mn^{3+} ions form a two-dimensional octa-kagomé lattice parallel to (001) (Figure 2c). The adjacent octa-kagomé layers are connected by [-Mn1-] chains. It is significant that there is a staircase-kagomé lattice composed of Mn^{2+} and Mn^{3+} parallel to (100) in the magnetic topological framework (Figure 2d). The shortest Mn–Mn distance in both [-Mn1-] and [-Mn3-] chains is 3.332(9) Å. However, the detailed connection mode of MnO_6 octahedra in [-Mn1-] chains are edge-sharing, whereas in [-Mn3-] chains it is corner-sharing. The Mn-O-Mn angles in [-Mn1-] and [-Mn3-] chains are 89.77(1)°/102.90(8)° and 127.61(5)°, respectively. The Mn2–Mn2 and Mn2–Mn3 distances in the octa-kagomé lattice are 3.150(0) Å and 3.069(6) Å, respectively, whereas the Mn1–Mn2 distance is 3.902(1) Å.

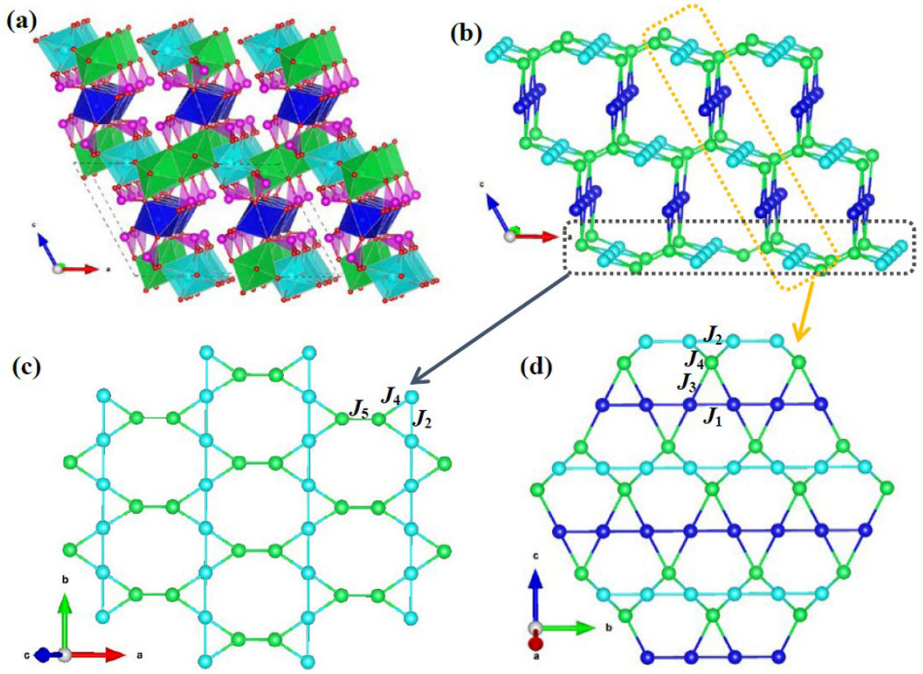

Figure 2. (**a**) The three-dimensional structure frameworks and (**b**) topological spin structures of $Mn_3O(SeO_3)_3$; (**c**,**d**) show the octa-kagomé and staircase-kagomé spin sublattices, respectively. Here the blue, green, light blue and pink polyhedra represent $Mn1O_6$, $Mn2O_6$, $Mn3O_6$ and SeO_3, respectively. Balls of the above colors represent Mn1, Mn2 and Mn3 ions, respectively.

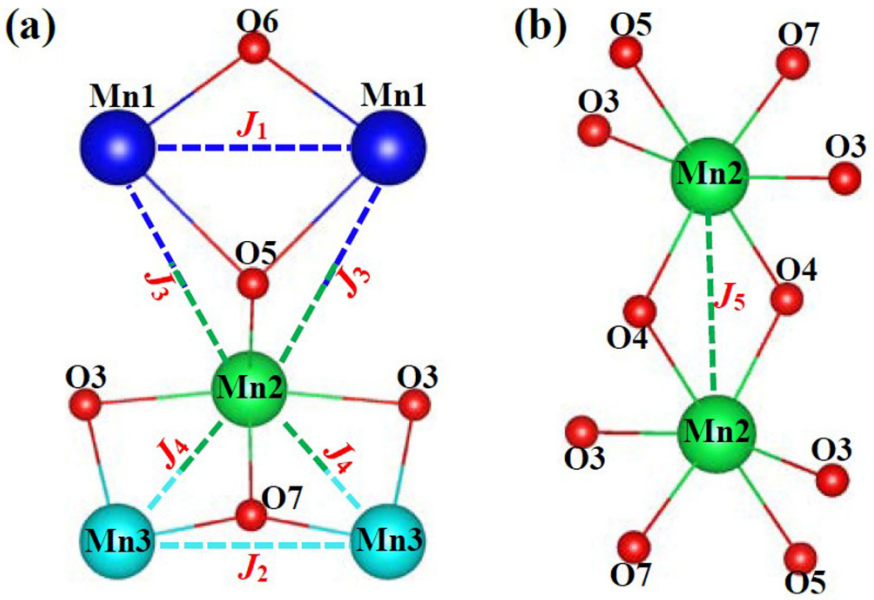

Figure 3. Detailed linkages of five main superexchange pathways in $Mn_3O(SeO_3)_3$. (**a**) indicates J_1 to J_4 and (**b**) indicates J_5, respectively.

Figure 4a shows the temperature dependence of magnetic susceptibility $\chi(T)$ of $Mn_3O(SeO_3)_3$ measured at 0.1 T. Magnetic susceptibility increases with decreasing temperature; two peaks can be observed at T_{N1}~4.5 K and T_{N2}~45 K., showing AFM transitions. At high temperature (80–300 K) inverse susceptibility $\chi^{-1}(T)$ follows the Curie–Weiss law with a Weiss temperature of $\theta = -8.89$ K and a Curie constant of $C = 11.03$ emu·mol^{-1}·K. The effective magnetic moment is calculated to be $\mu_{eff} = 5.42(3)$ μ_B, obtained by $\mu^2_{eff} = 8C/n$, where $n = 3$. This value of μ_{eff} is slightly smaller than the spin-only value of 5.91(6) μ_B

for Mn^{2+} ($3d^5$, high spin) and larger than the spin-only value of 4.89(9) μ_B for Mn^{3+} ($3d^4$, high spin). As Mn ions are mixed-valent, the theoretical magnetic moment of the titled compound is μ_{theo} = 5.25(9) μ_B obtained by the equation μ^2_{eff} = [μ^2_{eff} (Mn^{2+}) + 2μ^2_{eff} (Mn^{3+})]/3. The value of μ_{eff} is quite close to that of μ_{theo}, confirming that Mn ions in the structure are mixed valence. The negative value of θ suggests the presence of dominative AFM interactions between neighboring Mn ions. Figure S3 shows the χT-T curve, in which the value of χT decreases with decreasing temperature, which is characteristic of typical AFM interactions. As shown in Figure 4b, the heat capacity data of $Mn_3O(SeO_3)_3$ show a λ-type peak at T~45 K and a corner-type transition at 4.5 K, providing concrete evidence for the two long-range magnetic orderings observed in the magnetic susceptibility curves.

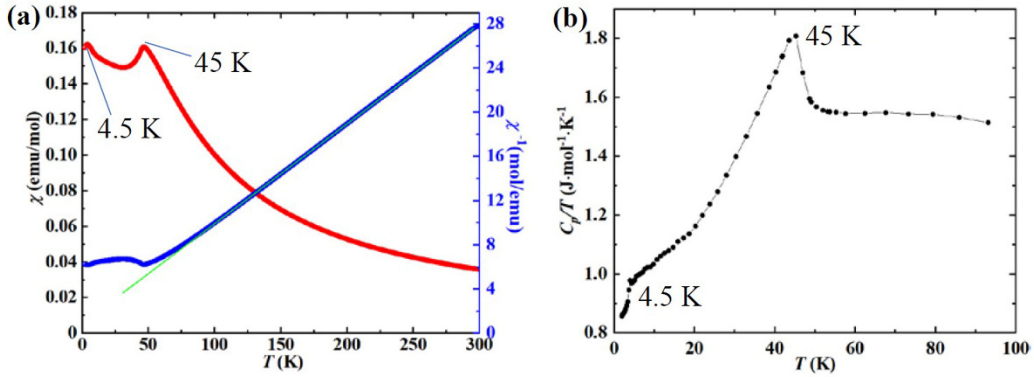

Figure 4. (**a**) The magnetic susceptibility $\chi(T)$ of $Mn_3O(SeO_3)_3$ and its reciprocal. (**b**) The heat capacity of $Mn_3O(SeO_3)_3$. The green solid line indicates Curie–Weiss fitting.

To further investigate the magnetic properties of the system, magnetization (M) as a function of applied field (H) was observed at 30 K and 2 K. As shown in Figure 5, at 30 K, magnetization increased linearly with increasing field, and did not saturate at 9 T. Furthermore, no hysteresis or remanent magnetization was observed. These features of the M–H curve suggest that the magnetic anomaly at T~45 K is the onset of an AFM ordering. At 2 K, the magnetization (M) shows a linear increase in magnetization at low field, indicative of a characteristic AFM ground state. A clear change in slope in the magnetization is observed at approximately 4.5 T, indicating field-induced magnetic transition. Furthermore, no hysteresis can be observed on the M–H curve.

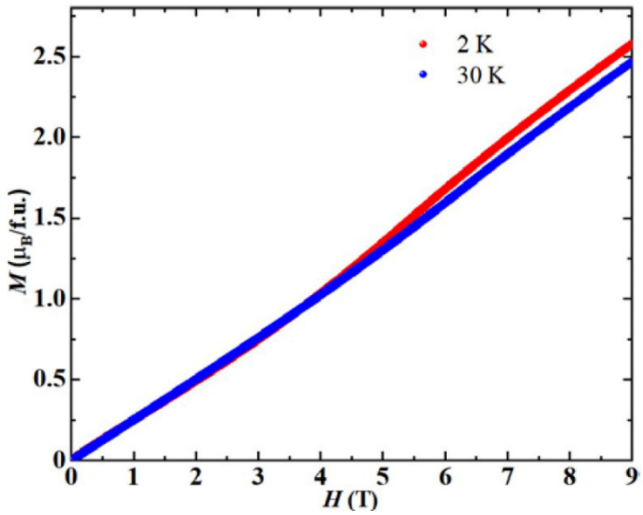

Figure 5. Isothermal magnetization (M) as a function of applied field (H) at 2 K and 30 K.

It is well-known that the magnetic properties of solid magnets are strongly related to their structural features. The three-dimensional manganese topological framework of $Mn_3O(SeO_3)_3$ is formed by the intersection of octa-kagomé lattices and staircase-kagomé lattices. Firstly, we know that the kagomé-like lattices containing equilateral or isosceles triangle sublattices may exhibit strong frustrated magnetic properties [19–21]. We note the value of frustration factor, $f = |\theta| / T_N \sim 0.20$, with Weiss temperature $\theta = -8.89$ K and Neel temperature $T_{N2} \sim 45$ K, ruling out spin frustration in the system. It is well known that primary magnetic interactions originate from the superexchange of Mn-O-Mn. A detailed description of superexchange interactions is shown in Figure 2c,d and itemized in Table 1; there are five main magnetic exchange interactions, numbered J_1–J_5, within the three-dimensional spin-lattice according to the Goodenough–Kanamori–Anderson rules (GKA rules) [22]. There are two isosceles triangular topological configurations composed by J_1–J_4 on the staircase-kagomé spin sublattice. According to the GKA rules, J_2 and J_3 are AFM interactions. J_1 and J_4 both have two Mn-O-Mn superexchange interactions, as the corresponding MnO_6 octahedra share their edges. In general, the spin exchange parameter, J, can be written as $J = J_{FM} + J_{AFM}$, where J_{FM} indicates ferromagnetic exchange and J_{AFM} indicates antiferromagnetic exchange ($J_{FM} > 0$ and $J_{AFM} < 0$) [23]. So, $J_1 = J_{1FM(O5)} + J_{1AFM(O6)}$, and the AFM interaction via O6 in J_1 is negligible; this means that $J_1 \approx J_{1FM(O5)} > 0$. Using the same analytical method, the spin exchange parameter, J_4, is ambiguous, as the magnitude of $J_{4AFM(O7)}$ is difficult to calculate. J_5 should be a weak AFM interaction. This analysis indicates that AFM interactions are dominant in the system, which is consistent with the negative value of θ. It is significant that the neighboring octa-kagomé sublattices are separated by [-Mn1-] chains and that the neighboring staircase-kagomé sublattices are connected by $[Mn_2O_{10}]$ dimers. It is safely said that these two long-range magnetic orders are driven by interlayer magnetic coupling. It is noteworthy that [-Mn1-] chains are composed of Mn^{2+} ions. If Mn^{2+} ions are replaced with nonmagnetic ions with a radius similar to Mn^{2+}, such as Mg^{2+} or Zn^{2+} [24], an octa-kagomé lattice composed of Mn^{3+} ions might form. The expected compounds may exhibit spin-liquid or other quantum physical properties [25,26]. Exploratory synthesis of related compounds is underway.

Table 1. Geometric parameters of dominant magnetic superexchanges in $Mn_3O(SeO_3)_3$ *.

J_1	d(Mn-O) (Å)	d(Mn-Mn) (Å)	Mn-O-Mn Angle (°)	Magnetism
J_1	Mn1-2.130(7)-O6-2.130(7)-Mn1 Mn1-2.361(4)-O5-2.361(4)-Mn1	3.332(9)	Mn1-O6-Mn1 ... $102.90(8)_{AFM\text{-}w}$ Mn1-O5-Mn1 ... $89.77(1)_{FM\text{-}S}$	FM
J_2	Mn3-1.857(1)-O7-1.857(1)-Mn3	3.332(9)	Mn3-O7-Mn3 ... $127.61(5)_{AFM\text{-}S}$	AFM
J_3	Mn1-2.361(4)-O5-2.278(1)-Mn2	3.902(1)	Mn1-O5-Mn2 ... $114.49(4)_{AFM\text{-}S}$	AFM
J_4	Mn2-2.049(5)-O3-2.310(4)-Mn3 Mn2-1.854(2)-O7-1.857(1)-Mn3	3.069(6)	Mn2-O3-Mn3 ... $89.29(7)_{FM\text{-}S}$ Mn2-O7-Mn3 ... $111.59(8)_{AFM\text{-}S}$	?
J_5	Mn2-1.896(5)-O4-2.169(5)-Mn2 Mn2-2.169(5)-O4-1.896(5)-Mn2	3.150(0)	Mn2-O4-Mn2 ... $101.34(9)_{AFM\text{-}w}$ × 2	AFM

* The S or W behind AFM or FM (in the Mn-O-Mn Angle (°) column) refers to the magnitude of the J value; S refers to strong and W refers to weak.

As shown in Figure 6, $Mn_3O(SeO_3)_3$ undergoes a slow weight gain of approximately 0.20% from 100 to 200 °C and a slow weight loss of approximately 0.40% from 300 to 400 °C. As the weight of the sample is only approximately 7 mg, slight weight gain/loss may be caused by instrument error. As the temperature rises, two successive steps of weight loss of approximately 57% occur from 450 to 630 °C, corresponding to the calculated 59% loss of $3SeO_2$. The 2% difference may also be caused by instrument error. Based on this analysis, the final residues of $Mn_3O(SeO_3)_3$ should be Mn_3O_4; however, this was difficult to characterize, as the residues melted in the Al_2O_3 crucible after being heated to 900 °C. We re-selected the sample and sintered it in a smooth quartz crucible at 800 °C in a nitrogen atmosphere for 10 min. We then scraped off the sintered product and performed powder X-ray diffraction analysis. As shown in Figure S4, the residue was confirmed as Mn_3O_4 (PDF #80-0382). This result is consistent with the decomposition characteristics of most manganese-based compounds.

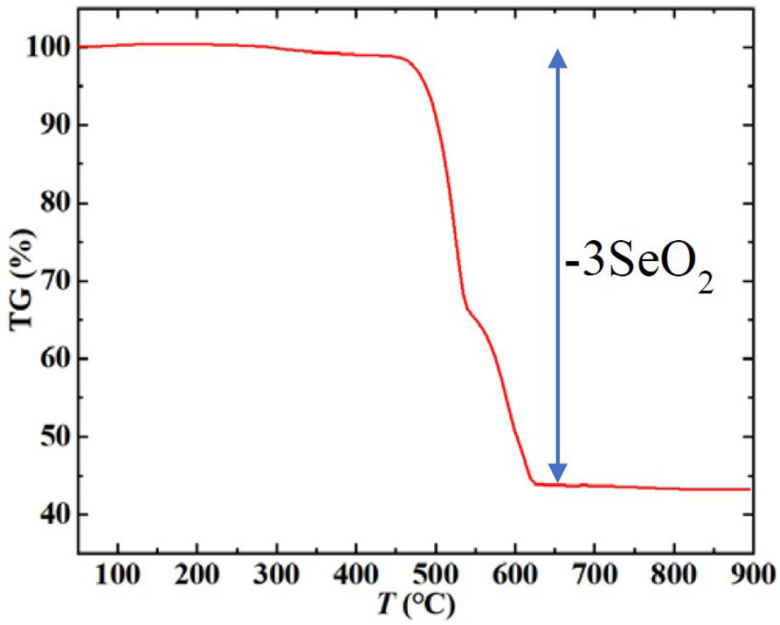

Figure 6. The thermogravimetric curve of $Mn_3O(SeO_3)_3$, which shows that the residual product of decomposition above 630 °C is Mn_3O_4.

4. Conclusions

A mixed-valence compound, $Mn_3O(SeO_3)_3$, was successfully synthesized using a conventional hydrothermal method. The reagent LiI acted as a mineralizer. $Mn_3O(SeO_3)_3$ was shown to have a channel structure with a three-dimensional magnetic topological framework formed by the intersection of octa-kagomé spin sublattices and staircase-kagomé spin sublattices. Magnetic and specific heat data confirmed that $Mn_3O(SeO_3)_3$ exhibits two successive long-range AFM orderings with T_{N1}~4.5 K and T_{N2}~45 K, and a field-induced spin–flop at a 4.5 T critical field at low temperature. Moreover, magnetic measurements confirmed that the ratio of Mn^{2+}/Mn^{3+} ions in this compound is 1:2, which is consistent with the structural analysis. The exploratory synthesis of Mg^{2+} or Zn^{2+} replaced compounds is in progress.

Supplementary Materials: The following supporting information can be downloaded at: https://www.mdpi.com/article/10.3390/ma15165773/s1, Figure S1. Single crystals of $Mn_3O(SeO_3)_3$ obtained by a conventional hydrothermal method. Figure S2. The oxygen-coordination environments for (a) Mn1, (b) Mn2, (c) Mn3, (d) Se1, (e) Se2 and (f) Se3 atoms in $Mn_3O(SeO_3)_3$. Figure S3. The variation in χT with the temperature of $Mn_3O(SeO_3)_3$. With the decreasing temperature, the value of χT decreases. Figure S4. Powder X-ray diffraction pattern for the final residues of $Mn_3O(SeO_3)_3$ after sintered at 800 °C for 10 min in nitrogen atmosphere.

Author Contributions: W.Z. and G.Q. conceived and designed the experiments. W.Z. prepared the materials and performed the XRD and magnetism testing. J.T. performed the thermogravimetric measurement. P.J. carried out the selection of pure phase crystals. W.Z., M.C. and G.Q. analyzed the data. W.Z. and G.Q. wrote the paper. M.C., J.T., P.J. and X.L. edited the paper. All authors discussed the results and commented on the manuscript. All authors have read and agreed to the published version of the manuscript.

Funding: This research was funded by the Hundreds of Talents program of Sun Yat-sen University and the Shenzhen Science and Technology Program (Grant No. RCBS20200714114820077).

Informed Consent Statement: Informed consent was obtained from all subjects involved in the study.

Data Availability Statement: Data is contained within the article or supplementary material.

Conflicts of Interest: The authors declare that they have no known competing financial interests or personal relationships that could have appeared to influence the work reported in this paper.

References

1. Varma, C.M. Mixed-valence compounds. *Rev. Mod. Phys.* **1976**, *48*, 219–238. [CrossRef]
2. Brown, D.B. *Mixed-Valence Compounds: Theory and Applications in Chemistry, Physics, Geology, and Biology*; Springer Science & Business Media: Berlin/Heidelberg, Germany, 2012.
3. Sleight, A.W. Chemistry of high-temperature superconductors. *Science* **1988**, *242*, 1519–1527. [CrossRef] [PubMed]
4. Uehara, M.; Mori, S.; Chen, C.H.; Cheong, S.W. Percolative phase separation underlies colossal magnetoresistance in mixed-valent manganites. *Nature* **1999**, *399*, 560–563. [CrossRef]
5. Tranquada, J.M. John Goodenough and the many lives of transition-metal oxides. *J. Electrochem. Soc.* **2022**, *169*, 010535. [CrossRef]
6. Saha, R.A.; Bandyopadhyay, A.; Schiesaro, I.; Bera, A.; Mondal, M.; Meneghini, C.; Ray, S. Colossal electroresistance response accompanied by metal-insulator transition in a mixed-valent vanadate. *Phys. Rev. B* **2021**, *104*, 045149. [CrossRef]
7. Wu, T.; Zhao, H.; Zhu, X.; Xing, Z.; Liu, Q.; Liu, T.; Gao, S.; Lu, S.; Chen, G.; Asiri, A.M.; et al. Identifying the origin of Ti^{3+} activity toward enhanced electrocatalytic N_2 reduction over TiO_2 nanoparticles modulated by mixed-valent copper. *Adv. Mater.* **2020**, *32*, 2000299. [CrossRef]
8. Chen, H.; Liu, Y.; Cai, T.; Dong, W.; Tang, L.; Xia, X.; Wang, L.; Li, T. Boosting photocatalytic performance in mixed-valence MIL-53(Fe) by changing Fe^{II}/Fe^{III} ratio. *ACS Appl. Mater. Inter.* **2019**, *11*, 28791–28800. [CrossRef]
9. Michel, C.; Hervieu, M.; Borel, M.M.; Grandin, A.; Deslandes, F.; Provost, J.; Raveau, B. Superconductivity in the Bi-Sr-Cu-O system. *Z. Phys. B* **1987**, *68*, 421–423. [CrossRef]
10. Raveau, B. Copper mixed valence concept: "Cu(I)–Cu(II)" in thermoelectric copper sulfides—an alternative to "Cu(II)–Cu(III)" in superconducting cuprates. *J. Supercond. Nov. Magn.* **2019**, *33*, 259–263. [CrossRef]
11. Zinzuvadiya, S.; Pandya, R.J.; Singh, J.; Joshi, U.S. Low field magnetotransport behavior of barium hexaferrite/ferromagnetic manganite bilayer. *J. Appl. Phys.* **2021**, *130*, 024102. [CrossRef]
12. Hasegawa, K.; Isobe, M.; Yamauchi, T.; Ueda, H.; Yamaura, J.; Gotou, H.; Yagi, T.; Sato, H.; Ueda, Y. Discovery of ferromagnetic-half-metal-to-insulator transition in $K_2Cr_8O_{16}$. *Phys. Rev. Lett.* **2009**, *103*, 146403. [CrossRef] [PubMed]
13. Lin, R.; Bak, S.M.; Shin, Y.; Zhang, R.; Wang, C.; Kisslinger, K.; Ge, M.; Huang, X.; Shadike, Z.; Pattammattel, A.; et al. Hierarchical nickel valence gradient stabilizes high-nickel content layered cathode materials. *Nat. commun.* **2021**, *12*, 2350. [CrossRef] [PubMed]
14. Ran, Q.; Zhao, H.; Hu, Y.; Hao, S.; Liu, J.; Li, H.; Liu, X. Enhancing surface stability of $LiNi_{0.8}Co_{0.1}Mn_{0.1}O_2$ cathode with hybrid core-shell nanostructure induced by high-valent titanium ions for Li-ion batteries at high cut-off voltage. *J. Alloy. Compd.* **2020**, *834*, 155099. [CrossRef]
15. Yu, X.; Tokunaga, Y.; Taguchi, Y.; Tokura, Y. Variation of topology in magnetic bubbles in a colossal magnetoresistive manganite. *Adv. Mater.* **2017**, *29*, 1603958. [CrossRef] [PubMed]
16. Wildner, M. Crystal structure of $Mn(II)Mn(III)_2O(SeO_3)_3$. *J. Solid State Chem.* **1994**, *113*, 252–256. [CrossRef]
17. Toby, B.H. EXPGUI, a graphical user interface for GSAS. *J. Appl. Crystallogr.* **2001**, *34*, 210–213. [CrossRef]
18. Momma, K.; Izumi, F. VESTA 3 for three-dimensional visualization of crystal, volumetric and morphology data. *J. Appl. Crystallogr.* **2011**, *44*, 1272–1276. [CrossRef]
19. Balents, L. Spin liquids in frustrated magnets. *Nature* **2010**, *464*, 199–208. [CrossRef]
20. Aidoudi, F.H.; Aldous, D.W.; Goff, R.J.; Slawin, A.M.; Attfield, J.P.; Morris, R.E.; Lightfoot, P. An ionothermally prepared S = 1/2 vanadium oxyfluoride kagome lattice. *Nat. Chem.* **2011**, *3*, 801–806. [CrossRef]
21. Chu, S.; McQueen, T.M.; Chisne, R.; Freedman, D.E.; Muller, P.; Lee, Y.S.; Nocera, D.G. A Cu^{2+} (S = 1/2) kagomé antiferromagnet: $Mg_xCu_{4-x}(OH)_6Cl_2$. *J. Am. Chem. Soc.* **2010**, *132*, 5570–5571. [CrossRef]
22. Goodenough, J.B. *Magnetism and the Chemical Bond*; John Wiley and Sons: New York, NY, USA, 1966.
23. Whangbo, M.H.; Koo, H.J.; Dai, D.; Jung, D. Effect of metal-ligand bond lengths on superexchange interactions in Jahn-Teller d^4 ion systems: Spin dimer analysis of the magnetic structure of Marokite $CaMn_2O_4$. *Inorg. Chem.* **2002**, *41*, 5575–5581. [CrossRef] [PubMed]

24. Shannon, R.D. Revised effective ionic radii and systematic studies of interatomic distances in halides and chalcogenides. *Acta Crystallogr. A* **1976**, *32*, 751–767. [CrossRef]
25. Peng, C.; Ran, S.-J.; Liu, T.; Chen, X.; Su, G. Fermionic algebraic quantum spin liquid in an octa-kagomé frustrated antiferromagnet. *Phys. Rev. B* **2017**, *95*, 075140. [CrossRef]
26. Tang, Y.; Peng, C.; Guo, W.; Wang, J.F.; Su, G.; He, Z. Octa-kagomé lattice compounds showing quantum critical behaviors: Spin gap ground state versus antiferromagnetic ordering. *J. Am. Chem. Soc.* **2017**, *139*, 14057–14060. [CrossRef] [PubMed]